Catalysis Letters
https://doi.org/10.1007/s10562-019-02799-3

Selective Oxidation of Glyoxal to Glyoxalic Acid by Air over Mesoporous Silica Supported Pd Catalysts

Junchi Liu[1] · Feng Qin[1] · Zhen Huang[1] · Liang Huang[1] · Zhenan Liao[1] · Hualong Xu[1] · Wei Shen[1]

Received: 3 February 2019 / Accepted: 15 April 2019

Abstract

A series of mesoporous silica (KIT-6, MCM-41 and SBA-15) supported Pd catalysts were successfully synthesized and applied for selective oxidation of glyoxal. All of these catalysts exhibited significantly higher activity than commercial Pd/C. Among them, Pd/KIT-6 exhibited the best activity and selectivity with 41.3% glyoxal conversion and 57.0% selectivity to glyoxalic acid. The better performance of Pd/KIT-6 was attributed to its three-dimensional mesoporous structure. The three-dimensional mesoporous structure of KIT-6 could enhance Pd dispersion, providing sufficient accessible active sites which improved the conversion of glyoxal. Meanwhile, the better mass transfer capability of Pd/KIT-6 allowed glyoxalic acid to leave the catalyst easily, reducing the probability of over-oxidation. The ratio of k_I (rate constant of initial oxidation reaction) to k_{II} (rate constant of over-oxidation) was compared among three catalysts. The k_I/k_{II} of Pd/KIT-6 (0.50) was higher than that of Pd/MCM-41 (0.39) and Pd/SBA-15 (0.34), which reflected its best selectivity from kinetic aspect.

Graphical Abstract

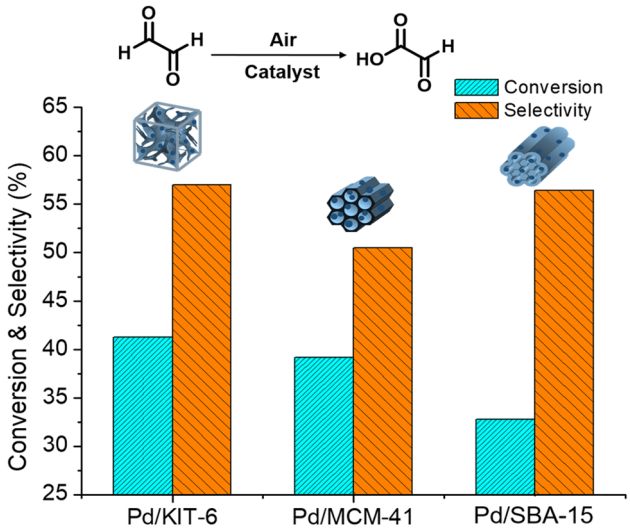

Keywords Selective catalytic oxidation · Glyoxal · Glyoxalic acid · Mesoporous silica supported Pd

✉ Wei Shen
wshen@fudan.edu.cn

[1] Department of Chemistry, Shanghai Key Laboratory of Molecular Catalysis and Innovative Materials, Laboratory of Advanced Materials, Collaborative Innovation Center of Chemistry for Energy Materials, Fudan University, Shanghai 200433, People's Republic of China

1 Introduction

Glyoxalic acid is a valuable fine chemical and an important intermediate of numerous products, such as flavor, perfume, cosmetics and drug modifiers, especially in the preparation of penicillin and vanillin [1–3]. Nowadays, glyoxalic acid is

Published online: 04 May 2019

industrially manufactured by glyoxal oxidation with nitric acid. However, this process produces large amounts of nitrogen oxides (NO_x), which causes severe potential environmental problems. It is therefore urgent to be substituted by green synthesis route. Direct selective oxidation of glyoxal to glyoxalic acid, using air as oxidant, is an attractive and environmentally-friendly route to solve these problems. Recently, some carbon supported noble metal catalysts, such as Pd/C, Pt/C and Au/C have been applied in the title reaction as active components [4–7]. Among them, Pd/C exhibited superior activity for selective oxidation of glyoxal under mild condition. However, there are still some challenges for Pd/C in this reaction. First, the most active monometallic Pd/C catalyst exhibits relative low activity with about 15% yield of glyoxalic acid after 20 h. By bimetallic modification, the Ru–Pd/C catalyst can reach around 20% yield of glyoxalic acid [4, 8, 9]. Besides, the product, glyoxalic acid, is easily over-oxidized to oxalic acid, which leads to low selectivity [10]. Therefore, there is a significant demand for development of new catalyst systems to achieve higher activity and selectivity.

Mesoporous silica (MS), as a kind of excellent catalytic supports with high surface area, ordered pore structure and flexible pore architecture [11, 12], is widely used in the heterogeneous catalysis [13–15]. In the past decades, various mesoporous silicas with tunable pore size have been synthesized, such as M41S family, SBA series and MSU-X. Their superior catalytic performance in photocatalysis reaction, selective oxidation reaction and organic synthesis was verified [16–18]. Karimi et al. [19] reported Pd immobilized on SBA-15 for the aerobic oxidation of alcohols. The Pd nanoparticles were well confined inside the channel of SBA-15 and they acted as active species for the aerobic oxidation of a wide range of alcohols. Afterwards, Parlett et al. [20, 21] found that Pd dispersed on SBA-16 and KIT-6 exhibited enhanced aerobic alcohol oxidation performance owing to their three-dimensional (3D) interconnected architecture. For the aerobic alcohol oxidation, the 3D architecture of MS supports led to the obvious enhancement of incorporated metal dispersion and mass transfer in liquid phase. Since these investigated oxidation reactions did not face the problem of severe over-oxidation, their work mainly focused on the promotion of conversion by the 3D mesoporous structure of supports.

Despite these excellent features of MS, to our knowledge, there is no report on MS supported Pd catalyst for selective oxidation of glyoxal to glyoxalic acid by air. Herein, we prepared a series of Pd/MS catalysts (Pd/KIT-6, Pd/MCM-41 and Pd/SBA-15) to investigate their catalytic performance. Compared with 2D architecture of MCM-41 and SBA-15, we speculated that the 3D architecture of KIT-6 could provide highly dispersed active sites, which were more accessible to reactant molecules. Meanwhile, its interconnected mesopore favored the mass transfer of reactants, which helped to reduce the chance of over-oxidation. Consequently, the dimensionality effect of supports on the catalytic activity and selectivity was investigated.

2 Experimental Sections

2.1 Synthesis of MS Supports

Mesoporous KIT-6, MCM-41 and SBA-15 were synthesized according to the literature [20, 22]. For KIT-6, 4.0 g Pluronic P123 was dissolved in 144 g water, 4.0 g Butan-1-ol and 7.9 g (35 wt%) hydrochloric acid with stirring at 40 °C. Then 8.6 g tetraethyl orthosilicate was added dropwise and stirred for 24 h. Subsequently, the mixture was aged at 100 °C for 24 h without stirring. The obtained suspension was filtered and washed with water, dried overnight before calcination at 550 °C for 6 h. For MCM-41, 4.0 g hexadecyltrimethylammonium bromide was dissolved in 200 g water and 15.9 g (25 wt%) aqueous ammonia with stirring at 25 °C. Then 16.7 g of tetraethyl orthosilicate was added dropwise and stirred for 1 h. The obtained suspension was filtered, washed with water and dried overnight before calcination at 550 °C for 6 h. For SBA-15, 4.0 g Pluronic P123 was dissolved in 127 g water and 85 g of 4 M hydrochloric acid with stirring at 35 °C. Then 11.3 g of tetraethyl orthosilicate was added dropwise and stirred for 20 h. The obtained suspension was filtered and washed with water, dried overnight before calcination at 550 °C for 6 h samples.

2.2 Preparation of Pd/MS Catalysts

The Pd (1 wt%)/MS catalysts were prepared by impregnation method in acetic solution. 0.011 g $Pd(OAc)_2$ was dissolved in 50 mL acetic solution. The synthesized MS support (0.50 g) was then added to the above solution and stirred for 4 h at 50 °C. After that, the solvent in suspension solution was vaporized under a vacuum in a rotary evaporator. The obtained precursor was then dried at 90 °C overnight. Finally, the dried powder was calcined in air at 350 °C for 3 h, followed by reduction at 350 °C for 3 h in hydrogen. These catalysts were denoted as Pd/SBA-15, Pd/MCM-41 and Pd/KIT-6.

2.3 Characterization

Nitrogen adsorption and desorption isotherms were performed by Micromeritics ASAP2020. Samples were degassed at 200 °C before measurements. The specific surface areas were calculated by the BET equation. The pore diameters and volumes were determined by applying the

Barrett–Joyner–Halenda (BJH) method to the desorption branch of the isotherms.

Small-angle X-ray scattering (SAXS) measurements were taken on a Nanostar U small-angle X-ray scattering system (Bruker, Germany) using $Cu_{K\alpha}$ radiation (40 kV, 35 mA). Wide-angle X-ray diffraction (XRD) patterns were recorded on a Bruker AXS D8 diffractometer ($Cu_{K\alpha}$ radiation, $\lambda = 0.154$ nm), operated at 40 kV and 40 mA.

High resolution TEM images were recorded on an FEI Tecnai F20 field emission gun (FEG-)TEM operating at 200 kV equipped with a Gatan Orius SC600A camera. Images were analyzed by ImageJ 1.41 and the mean Pd particle diameters were calculated by analyzing 100–150 particles for each sample using Nano Measurer program.

CO pulse chemisorption (Autochem II 2920, Micromeritics Co., USA) measurements were used to measure the Pd dispersion. Samples were outgassed at 150 °C under flowing hydrogen (20 mL/min) for 1 h, followed by flowing He (20 mL/min) for 1 h before analysis at room temperature. This reduction temperature was much lower than the process during catalysts synthesis thus did not induce additional sintering of Pd particles.

2.4 Catalytic Performance

The catalytic reaction was performed in a glass flask. 100 mL (100 mmol/L) glyoxal solution and 100 mg catalyst were added in the reactor and then heated at 40 °C with constant stirring rate of 1000 rpm. The pH of the reaction mixture was constantly measured by a pH electrode. In order to keep the pH value at 7.2, a solution of 0.3 mol/L Na_2CO_3 was added into the reaction mixture to neutralize the generated acid by an automatic titration device. Air, as oxidant, was bubbled through the solution with a constant flow rate of 400 mL/min. In recycle studies, the same reaction conditions were performed except using recovered catalysts.

The reaction products were sampled after removal of catalysts, and the components of filtrate were quantified by Shimadzu HPLC, on a Phenomenex Synergi 4u Hydro-RP 80A column, heated at 25 °C. The injection volume was 20 µL, and a sulfuric acid solution (pH 2.7) was used as the mobile phase with a flux of 1 mL/min. The products were detected at 212 nm on a UV–Vis Spectra System 6000 LP photodiode array detector.

The main catalytic oxidation pathways are presented in Scheme 1. Because glycolic acid was formed from Cannizzaro dismutation of glyoxal, which depended only on the pH of reaction mixture and not on the catalyst. According to literature [9, 10], the corrected conversion (X^* = conversion without considering glycolic acid, %) and corrected selectivity (S^*, %) can be used to compare the natural properties of catalysts, defined as follows:

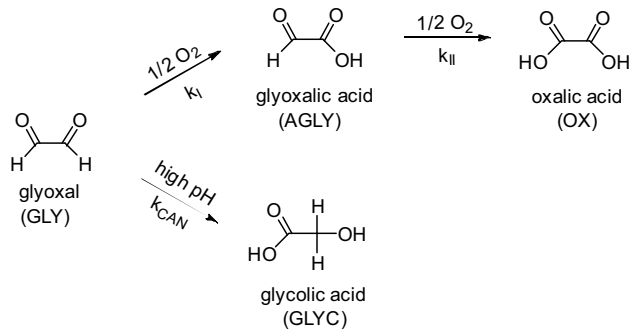

Scheme 1 Reaction pathways and corresponding products of glyoxal oxidation by air

$$Y = \frac{C_{\text{product}}}{C_{\text{GLY at } t=0}}$$

$$X^*_{\text{GLY}} = Y_{\text{AGLY}} + Y_{\text{OX}}$$

$$S^*_{\text{AGLY}} = \left(Y_{\text{AGLY}}/X_{\text{GLY}}\right) \times 100$$

3 Results and Discussion

3.1 Catalyst Characterization

SAXS patterns of these MS supports are shown in Fig. 1a. The SAXS results indicated the successful synthesis of KIT-6, MCM-41 and SBA-15. For KIT-6, it displayed a strong peak and a hump arising from (211) and (220) reflections. This pattern demonstrated that the prepared support had a well-ordered mesoporous structure, which belonged to the 3D cubic *Ia3d* space group. For MCM-41 and SBA-15, both of them exhibited one well-resolved peak and other two peaks, indexed as (100), (110) and (200) reflections, respectively. These distinct peaks of MCM-41 and SBA-15 corresponded to an ordered, 2D hexagonal mesophase of *P6mm*. Wide-angle XRD patterns of these Pd/MS catalysts are shown in Fig. 1b. All of them showed a broad peak at 22.2° attributed to the amorphous silica in pore wall. The other two sharp peaks at 40.2° and 46.6° were indexed as (111) and (200) planes of metallic Pd crystallites, and there was no PdO phase detected over all catalysts. The Pd diffraction peak of Pd/SBA-15 was the highest due to its large particle size among these catalysts. Compared with Pd/SBA-15 and Pd/MCM-41, Pd/KIT-6 displayed a broad diffraction peak of metallic Pd, implying that the 3D mesoporous structure of KIT-6 effectively promoted the dispersion of Pd with smaller particle size.

The nitrogen sorption isotherms of three MS supports at different stages (prior to depositing Pd, after deposition and

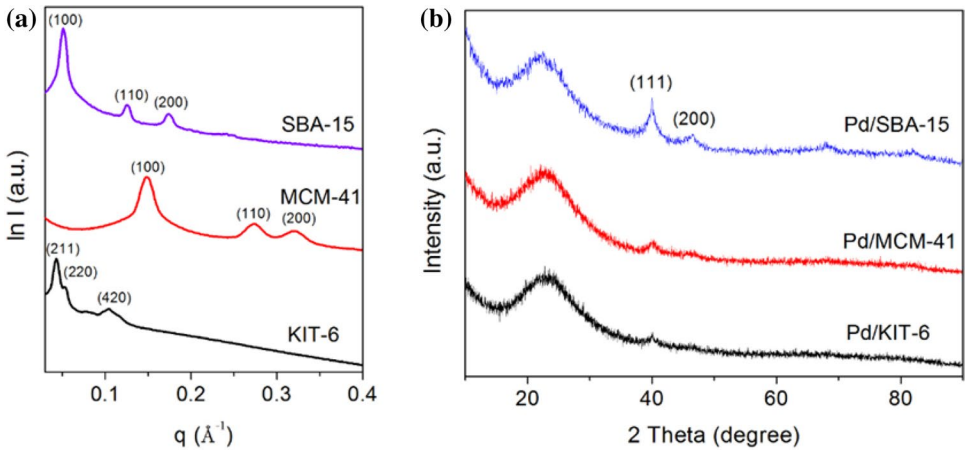

Fig. 1 **a** SAXS patterns of KIT-6, MCM-41 and SBA-15 supports; **b** wide-angle XRD patterns of Pd/KIT-6, Pd/MCM-41 and Pd/SBA-15 catalysts

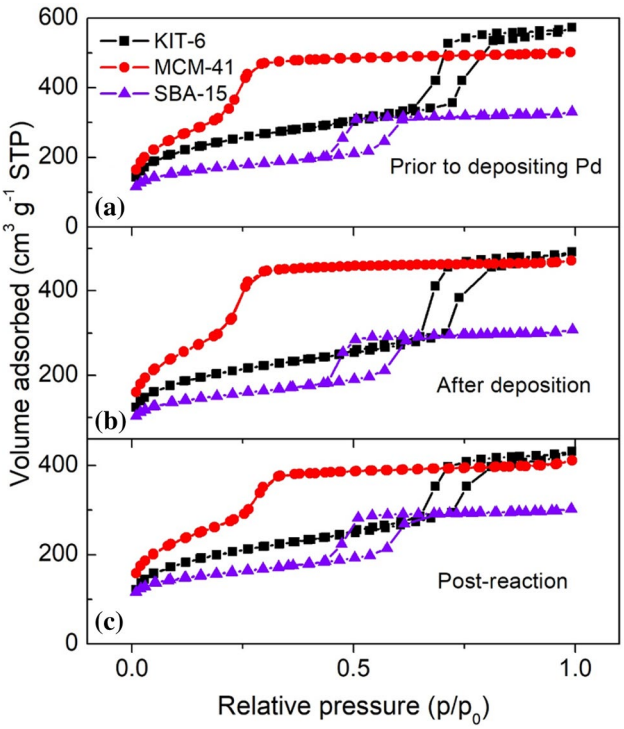

Fig. 2 Nitrogen adsorption–desorption isotherms of MS supports: *a* prior to depositing Pd, *b* after deposition, *c* post-reaction

post-reaction) are shown in Fig. 2. All samples demonstrated type IV isotherms according to IUPAC classification, and the isotherms of each sample were in good agreement with previous reports [21, 23–25]. For MCM-41 support without loading, the adsorption and desorption branches coincided and no hysteresis loops were observed. These isotherms exhibited sharp increase in the nitrogen uptake over a narrow range of $p/p_0 = 0.2–0.35$ due to the capillary condensation inside the mesopores. KIT-6 and SBA-15 showed typical H_1-type hysteresis arising from ordered mesoporous architecture. The BJH pore size distributions of all MS supports were in the mesoporous region with pore diameters 7.1 nm, 3.3 nm and 5.0 nm for KIT-6, MCM-41 and SBA-15, respectively. Their specific surface areas were consistent with literature values for parent MS [25, 26]. Textual properties of these MS supports before and after Pd impregnation are listed in Table 1. The types of isotherms, hysteresis and mean mesoporous diameters were almost unchanged after loading of Pd. Impregnation of Pd systematically depressed the surface area and pore volume, which reflected the partial blockage of the mesopores. Besides, the isotherms of all catalysts did not change obviously after reaction, indicating that the mesoporous structure of catalyst was well maintained during the oxidation of glyoxal.

Table 1 Textural properties of as-prepared MS supports and corresponding Pd/MS catalysts

Sample	S_{BET} (m^2/g)	Pore volume (cm^3/g)	Pore diameter (nm)	Dispersion of Pd[a] (%)	d_{Pd} (nm)	
					CO chem.[a]	STEM[b]
KIT-6	847	0.89	7.1			
Pd/KIT-6	715	0.76	7.0	49	2.5	2.5
MCM-41	1679	0.69	3.3			
Pd/MCM-41	1453	0.61	3.1	40	2.8	2.9
SBA-15	579	0.47	5.0			
Pd/SBA-15	505	0.44	4.8	30	3.8	4.0

[a]Dispersion of Pd and d_{Pd} were calculated from CO chemisorption

[b]d_{Pd} was calculated by STEM analysis

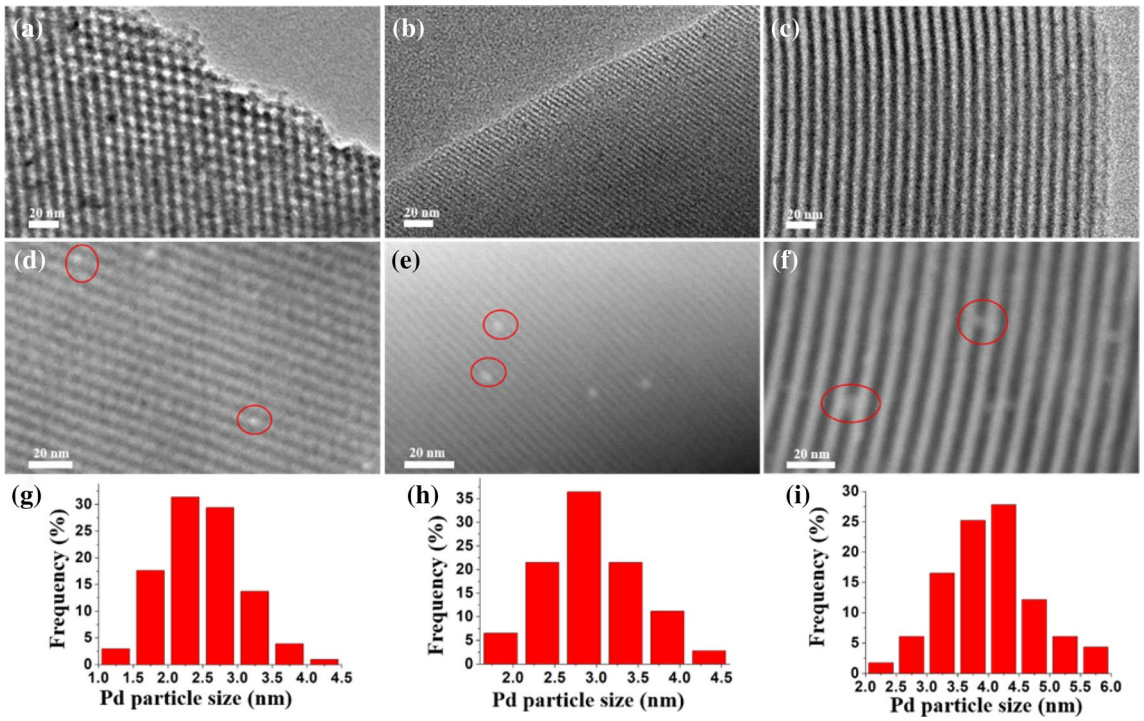

Fig. 3 Bright-field HRTEM images: **a** Pd/KIT-6, **b** Pd/MCM-41, **c** Pd/SBA-15; HAADF-STEM images: **d** Pd/KIT-6, **e** Pd/MCM-41, **f** Pd/SBA-15; Pd particle size distributions: **g** Pd/KIT-6, **h** Pd/MCM-41, **i** Pd/SBA-15. Analyses based upon 100–150 particles

The representative bright-field high-resolution TEM (HRTEM) and high-angle annular dark-field (HAADF)-STEM of these prepared Pd/MS catalysts are shown in Fig. 3. The HRTEM images clearly illustrated the retention of ordered and long parallel channels of Pd/MCM-41 and Pd/SBA-15 as well as cubic packed pore structure of Pd/KIT-6. This suggested that impregnation of Pd did not change the ordered mesoporous structure of MS supports. HAADF-STEM was used to observe the size distribution of Pd by analyzing 100–150 particles for each sample, and the Pd particles (brighter spots labeled by red circles) were well dispersed throughout all MS supports with mean particle size of 2.5 nm, 2.9 nm and 4.0 nm for Pd/KIT-6, Pd/MCM-41 and Pd/SBA-15, respectively. For Pd/MCM-41 and Pd/SBA-15, it could be observed that Pd species existed as nanorods (appeared as light, necklace-like objects along the channels) and nanoparticles. However, Pd species of KIT-6 appeared as spherical shape in the 3D mesopore.

The difference of Pd dispersion on these MS supports was also tested by CO chemisorption, from which, assuming a CO:$Pd_{surface}$ stoichiometry of 2:1 [27–29]. The dispersion of Pd decreased in the order of Pd/KIT-6 > Pd/MCM-41 > Pd/SBA-15. It indicated that KIT-6 support possessed the smallest Pd particle size, consistent with wide-angle XRD and HRTEM measurements. These results revealed that increasing mesopore interconnectivity and surface area of MS both

Table 2 Catalytic results of glyoxal oxidation over Pd/KIT-6, Pd/MCM-41 and Pd/SBA-15 catalysts

Catalysts	Reaction time (h)	X^*_{GLY} (%)	S^*_{AGLY} (%)	Y_{AGLY} (%)
Pd/KIT-6	5	16.5	81.2	13.4
	10	30.4	68.1	20.7
	15	41.3	57.0	23.5
	20	48.9	48.7	23.8
Pd/MCM-41	5	14.8	81.8	12.1
	10	28.0	65.7	18.4
	15	39.2	50.5	19.8
	20	47.1	45.2	21.3
Pd/SBA-15	5	10.3	86.4	8.9
	10	19.7	71.6	14.1
	15	32.8	56.4	18.5
	20	37.0	49.7	18.4
Pd/C	20	5.5	76.4	4.2
Pd/C [5]	20	3.8	81.2	3.1
Pd/C [8]	20	7.4	57.0	4.3
Bi–Pd/C [9]	20	26.3	54.3	14.3
Ru–Pd/C [4]	20	37.6	54.5	20.5

Reaction condition: 40 °C, 100 mg catalyst, 100 mL glyoxal (100 mmol/L), 1000 rpm of stirring rate

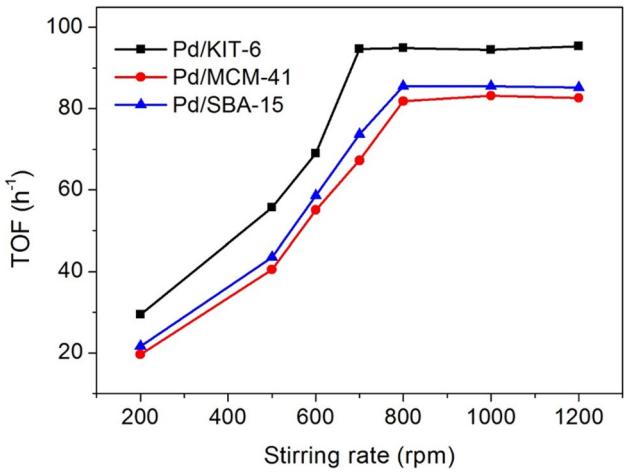

Fig. 4 Effect of stirring rate on turnover frequency (TOF) toward glyoxal oxidation of Pd/KIT-6, Pd/MCM-41 and Pd/SBA-15 after 1 h. Reaction conditions: 40 °C, 100 mg catalyst and 10 mmol glyoxal

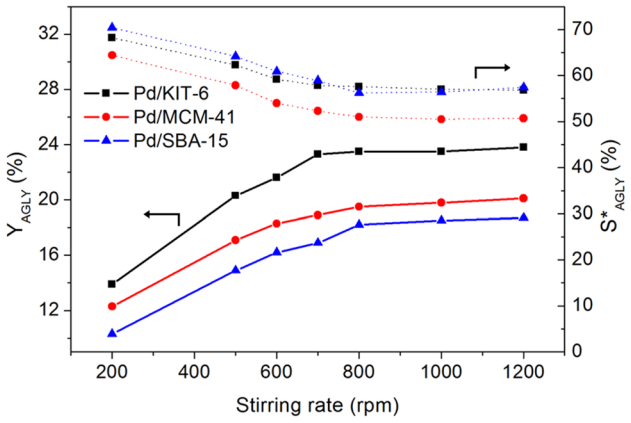

Fig. 5 Effect of stirring rate on catalytic performance toward glyoxal oxidation of Pd/KIT-6, Pd/MCM-41 and Pd/SBA-15 after 15 h. Reaction conditions: 40 °C, 100 mg catalyst and 10 mmol glyoxal

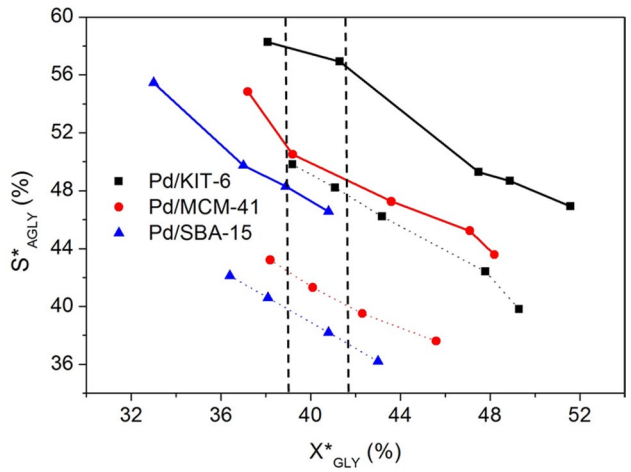

Fig. 6 S^*_{AGLY} against X^*_{GLY} under 500 rpm and 1000 rpm: the solid lines represent 1000 rpm of stirring rate and the dotted lines represent 500 rpm of stirring rate. Reaction conditions: 40 °C, 100 mg catalyst and 10 mmol glyoxal

helped to enhance the dispersion of Pd with smaller particle size.

3.2 Catalytic Performance

The catalytic performances of the synthesized Pd/MS catalysts and commercial Pd/C (J&K Scientific Ltd) catalyst were tested for selective oxidation of glyoxal by air, and the results are listed in Table 2. The results indicated that catalytic activity was very sensitive to supports. Compared with 5.5% glyoxal conversion after 20 h for Pd/C catalyst, three Pd/MS catalysts had at least 6 times higher activity than Pd/C in this reaction. To further investigate the catalytic behaviors of Pd/MS catalysts, their catalytic activity under different reaction time was also measured. For all Pd/MS catalysts, with extension of reaction time, the conversion of glyoxal increased and the selectivity of glyoxalic acid (AGLY) decreased. The yield of AGLY approximately reached the maximum at 15 h. It implied that glyoxalic acid was easily over-oxidized to oxalic acid. Among these catalysts, Pd/KIT-6 exhibited the best catalytic performance with 41.3% glyoxal conversion and 57.0% selectivity to AGLY after 15 h. Pd/MCM-41 exhibited 39.2% glyoxal conversion and 50.5% selectivity to AGLY after 15 h, which were both lower than those of Pd/KIT-6. Although Pd/SBA-15 attained similar selectivity with Pd/KIT-6, 32.8% glyoxal conversion was lower than 41.3% of Pd/KIT-6. Therefore, Pd/KIT-6 catalyst achieved higher conversion and selectivity at the same time. In addition, the catalytic activity of Pd/KIT-6 also exceeded those reported Pd-based catalysts.

In previous reports, KIT-6 supported Pd catalyst can improve the aerobic reaction rate of alcohols by its unique 3D mesoporous structure [20, 21]. This phenomenon was also observed in the oxidation of glyoxal. To further investigate the mass transfer of reactants in these Pd/MS catalysts, the values of turnover frequency (TOF) after 1 h were calculated and plotted against stirring rate in Fig. 4. For Pd/KIT-6, the plateau of TOF reached at 700 rpm, which was lower than 800 rpm of Pd/MCM-41 and Pd/SBA-15. This indicated that the diffusion of reactants over Pd/KIT-6 was better than those over Pd/MCM-41 and Pd/SBA-15. The 3D mesoporous structure of Pd/KIT-6 could favor the reactant molecules contacting active sites, leading to improved conversion of glyoxal. However, the 1D channels of Pd/MCM-41 and Pd/SBA-15, to some extent, hindered the reactant to access the active sites due to the longer diffusion pathway.

Catalytic activity of these Pd/MS catalysts under different stirring rate after 15 h is shown in Fig. 5. These results

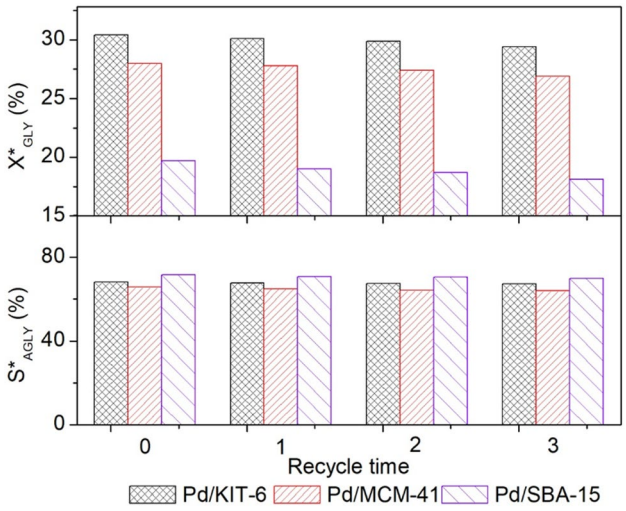

Fig. 7 Recycling tests of Pd/KIT-6, Pd/MCM-41 and Pd/SBA-15. Reaction condition: 40 °C, 10 h, and 10 mmol glyoxal

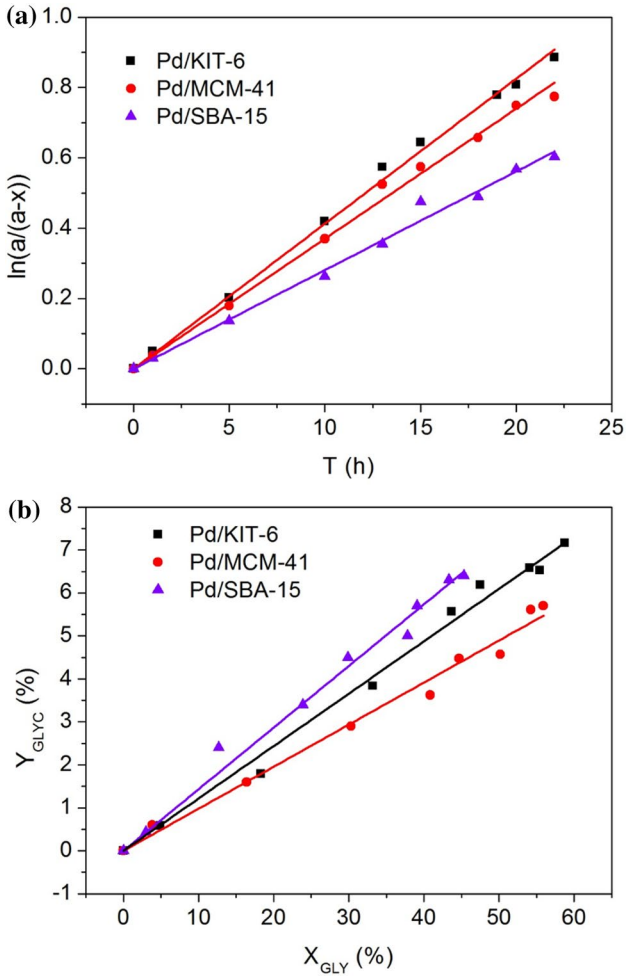

Fig. 8 General kinetics for Pd/KIT-6, Pd/MCM-41 and Pd/SBA-15 catalysts: **a** ln(*a*/(*a*–*x*)) as a function of time and **b** Y_{GLYC} as a function of X_{GLY}

indicated that the catalytic activity and selectivity were obviously affected by mixing state. When stirring rate was higher than 800 rpm, the external diffusion was eliminated for all catalysts, and further increase of stirring rate had no effect on activity and selectivity. To investigate the effect of mixing state on selectivity, the selectivity against conversion under 500 rpm and 1000 rpm is shown in Fig. 6. With the increase of conversion, selectivity decreased. It was observed that all catalysts achieved higher selectivity under higher stirring rate. Meanwhile, Pd/KIT-6 exhibited higher selectivity between 500 and 1000 rpm. It suggested that the selectivity of this consecutive reaction was obviously influenced by diffusion condition. Due to the poor diffusion under 500 rpm of stirring rate, the oxidized product (glyoxalic acid) might be difficult to depart from reaction region to solution, thus it would be over-oxidized to oxalic acid on the active sites. Pd/KIT-6 with 3D mesoporous structure exhibited excellent capability to facilitate the diffusion of product, resulting in higher selectivity under the same conversion. Besides, it was also obvious that Pd/KIT-6 had a higher conversion when the three catalysts reached the same selectivity.

To test the stability of these heterogenous catalysts, four consecutive runs were carried out. After 10 h reaction, catalysts were collected and reused for a new batch. Recycling results of the three catalysts are displayed in Fig. 7. The conversion and selectivity of these catalysts showed a slight decrease after four consecutive runs, which indicated the good stability of three Pd/MS catalysts.

3.3 Kinetic Study

In order to better reflect the differences among the three catalysts, kinetic study was also performed. Catalytic process is presented in Scheme 1. k_I represented the initial oxidation rate of glyoxal to glyoxalic acid and k_{II} represented the over-oxidation rate of glyoxalic acid to oxalic acid. k_{CAN} represented the dismutation reaction rate of glyoxal. Thus, k_{exp} ($k_{exp}=k_I+k_{CAN}$) represented the consumption rate of glyoxal. To measure the reaction kinetics, external diffusion limitation was eliminated under 1000 rpm according to above discussion. Derivation process of the kinetics was the same as literature based on first-order reaction hypotheses [4, 10].

$$k_{exp} \times t = \ln\left(a/(a-x)\right), k_{CAN}/k_{exp} = Y_{GLYC}/X_{GLY}$$

with $a=1$, $x=X_{GLY}/100$.

Thus k_{exp}, k_{CAN} and k_I ($k_I=k_{exp}-k_{CAN}$) could be obtained from these fitted lines, shown in Fig. 8. These linear plots implied that there was no obvious deactivation or metal leaching for all catalysts, and the calculated values of rate constants are listed in Table 3. In all cases, the similar values

Table 3 Values of first-order rate constants (h^{-1}) for Pd/KIT-6, Pd/MCM-41 and Pd/SBA-15 catalysts

	Catalysts		
	Pd/KIT-6	Pd/MCM-41	Pd/SBA-15
k_{exp}	0.041	0.037	0.028
k_{CAN}/k_{exp}	0.122	0.098	0.143
k_{CAN}	0.005	0.004	0.004
k_I	0.036	0.033	0.024
k_{II}	0.072	0.083	0.070
k_I/k_{II}	0.50	0.39	0.34

of k_{CAN} proved that the glycolic formation was independent of catalyst. As for k_I, it was obvious that Pd/KIT-6 possessed the highest value with 0.036 h^{-1}, demonstrating its superior activity to 2D architecture supports of Pd/MCM-41 and Pd/SBA-15 with k_I equal to 0.033 h^{-1} and 0.024 h^{-1}, respectively. Compared with Pd/SBA-15, the k_I of Pd/KIT-6 increased by 50%, which implied an obvious improvement of reaction rate. The highest k_I of Pd/KIT-6 might be ascribed to its 3D mesoporous structure, which provided sufficient active sites and favored the contact between active sites and reactant molecules. However, for the same 2D architecture, Pd/MCM-41 exhibited a higher value of k_I than Pd/SBA-15, probably due to its better Pd dispersion.

In order to reflect the degree of over-oxidation, the reaction rate of k_{II} was calculated as follows:

$$dC_{AGLY}/dt = k_I \times C_{GLY} - k_{II} \times C_{AGLY},$$

$$\Rightarrow dC_{AGLY}/dt = k_I \times a \times \exp(-k_{exp} \times t) - k_{II} \times C_{AGLY},$$

The solution of this differential equation was given by the software of Mathematica.

$$C_{AGLY} = (k_I \times a \times \exp(-k_{exp} \times t))/(k_{II} - k_{exp}) - (k_I \times a)/(k_{II} - k_{exp}) \times \exp(-k_{II} \times t)$$

Therefore, k_{II} reflected the over-oxidation rate and k_I/k_{II} could be used to compare the selectivity of different catalysts. The lower value of k_I/k_{II} indicated that glyoxalic acid was slowly produced or easily over-oxidized, leading to lower selectivity. The experimental plots of $Y_{AGLY}[t]$ and fitting curve of corresponding catalysts are displayed in Fig. 9. All fitting curves were well fitted with the experimental results, which implied that the obtained values of k_{II} were reliable. Both the values of k_{II} and k_I/k_{II} are also listed in Table 3.

In all cases, the value of k_{II} was higher than k_I, which confirmed that glyoxalic acid was easily over-oxidized to oxalic acid. For Pd/MCM-41 and Pd/SBA-15, the higher value of k_I corresponded to higher value of k_{II}, indicating that accelerating the reaction activity would also improve the reaction rate of over-oxidation. Taken together, Pd/KIT-6 possessed

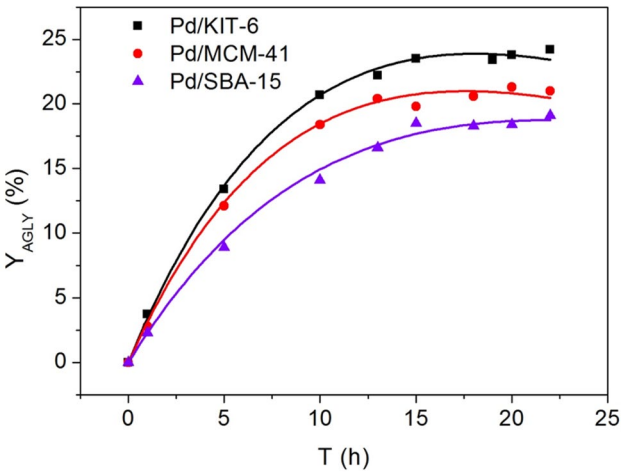

Fig. 9 General kinetics for Pd/KIT-6, Pd/MCM-41 and Pd/SBA-15 catalysts: Y_{AGLY} as a function of time

the highest value of k_I and relative low value of k_{II}, which were both beneficial to this reaction. The value of k_I/k_{II} was used to intuitively reflect the selectivity difference among these catalysts. The calculated k_I/k_{II} of Pd/KIT-6 was 0.50, which was obviously higher than 0.39 of Pd/MCM-41 and 0.34 of Pd/SBA-15. Compared with Pd/MCM-41, the k_I/k_{II} of Pd/KIT-6 increased by 28%, indicating an improvement of selectivity. This reflected the higher selectivity of Pd/KIT-6 from another aspect. Due to the 3D mesoporous architecture of KIT-6, the catalyst provided sufficient active sites, which were more accessible to reactants. Meanwhile, the oxidation product could also diffuse from catalyst to solution easily thanks to its better mass transfer capability. Therefore, the 3D mesoporous structure of Pd/KIT-6 provided an efficient way to improve the conversion and avoid over-oxidation at the same time.

4 Conclusions

Three series of Pd/MS catalysts have been synthesized and applied for selective oxidation of glyoxal by air under mild condition. Among these catalysts, Pd/KIT-6 exhibited higher catalytic activity and selectivity than those of Pd/MCM-41 and Pd/SBA-15. It was found that KIT-6 with 3D mesoporous structure enhanced Pd dispersion, making the active sites on Pd particles more accessible to reactants. Such an effect was reflected by the higher oxidation rate of

k_I. On the other hand, the 3D mesoporous structure of KIT-6 with better mass transfer capability allowed the product molecules to depart from catalysts to solution phase easily, which reduced the probability of over-oxidation side reaction. This advantage could also be confirmed by the relative low over-oxidation rate of k_{II}. These conclusions might also apply to other catalysts, and similar strategies could be developed for other liquid phase oxidations to achieve higher conversion and selectivity.

Acknowledgements This work was supported by the Shanghai Science and Technology Committee (Grant No. 14DZ2273900).

Compliance with Ethical Standards

Conflict of interest All authors declare that they have no conflict of interest.

References

1. Alardin F, Ruiz P, Delmon B, Devillers M (2018) Appl Catal A 215:125–136
2. Li K, Frost JW (1998) J Am Chem Soc 120:10545–10546
3. Meester WJN, Maarseveen JHV, Schoemaker HE, Hiemstra H, Rutjes FPJT (2003) Eur J Org Chem 1:2519–2529. https://doi.org/10.1002/ejoc.200200714
4. Deffernez A, Hermans S, Devillers M (2005) Appl Catal A 282:303–313
5. Hermans S, Thiltges F, Deffernez A, Devillers M (2012) Catal Lett 142:521–530
6. Jia ML, Liu CX, Wang J, Bao S, Bao Z (2014) Kinet Catal 55:671–675
7. Hermans S, Devillers M (2005) Catal Lett 99:55–64
8. Deffernez A, Hermans S, Devillers M (2007) J Phys Chem C 111:9448–9459
9. Alardin F, Delmon B, Ruiz P, Devillers M (2000) Catal Today 61:255–262
10. Alardin F, Wullens H, Hermans S, Devillers M (2005) J Mol Catal A 225:79–89
11. Zhao DY, Feng JL, Huo QS, Melosh N, Fredrickson GH, Chmelka BF, Stucky GD (1997) Science 279:548–552
12. Kleitz F, Choi SH, Ryoo R (2003) Chem Commun 17:2136–2137
13. Jiao F, Frei H (2009) Angew Chem Int Ed 48:1841–1844
14. Crudden CM, Sateesh M, Lewis R (2005) J Am Chem Soc 127:10045–10050
15. Kim SW, Son SU, Lee SI, Hyeon T, Chung YK (2000) J Am Chem Soc 122:1550–1551
16. Zhu K, Hu J, Richards R (2005) Catal Lett 100:195–199
17. Belhekar AA, Awate SV, Anand R (2002) Catal Commun 3:453–458
18. Naik B, Hazra S, Prasad VS, Ghosh NN (2011) Catal Commun 12:1104–1108
19. Karimi B, Abedi S, Clark JH, Budarin V (2006) Angew Chem Int Ed 118:4894–4897
20. Parlett CMA, Bruce DW, Hondow NS, Lee AF, Wilson K (2011) ACS Catal 1:636–640
21. Parlett CMA, Bruce DW, Hondow NS, Newton MA, Lee AF, Wilson K (2013) ChemCatChem 5:939–950
22. Cai Q, Lin WY, Xiao FS, Pang WQ, Chen XH, Zou BS (1999) Microporous Mesoporous Mater 32:1–15
23. Mastalir Á, Rác B, Király Z, Molnár Á (2007) J Mol Catal A 264:170–178
24. Sonwane CG, Bhatia SK (1999) Langmuir 15:2809–2816
25. Grün M, Unger KK, Matsumoto A, Tsutsumi K (1999) Microporous Mesoporous Mater 27:207–216
26. Li C, Zhang Q, Wang Y, Wan H (2008) Catal Lett 120:126–136
27. Marx S, Krumeich F, Baiker A (2011) J Phys Chem C 115:8195–8205
28. Cabilla GC, Bonivardi AL, Baltanás MA (1998) Catal Lett 55:147–156
29. Canton P, Menegazzo F, Polizzi S, Pinna F, Pernicone N, Riello P, Fagherazzi G (2003) Catal Lett 88:141–146